symmetry

MDPI

Article

Hysteretic Loops in Correlation with the Maximum Dissipated Energy, for Linear Dynamic Systems

Polidor Bratu

Research Institute for Construction Equipment and Technology—ICECON S.A., 021652 București, Romania; icecon@icecon.ro; Tel.: +40-021-202-5500

Received: 17 December 2018; Accepted: 21 February 2019; Published: 2 March 2019

Abstract: This paper presents the outcomes of the theoretical and experimental research carried out on a real model at natural scale using Voigt–Kelvin linear viscoelastic type m, c, and k models excited by a harmonic force $F(t) = F_0\ sin\omega t$, where F_0 is the amplitude of the harmonic force and ω is the excitation angular frequency. The linear viscous-elastic rheological system (m, c, k) is characterized by the fact that the c linear viscous damping—and, consequently, the fraction of the critical damping ζ—may be changed so that the dissipated energy can reach maximum $W_d^{\max}$ values. The optimization condition between the $W_d^{\max}$ maximum dissipated energy and the amortization $\zeta^0 = \pm\left(1-\Omega^2\right)/2\Omega$ modifies the structure of the relation $F = F(x)$, which describes the elliptical hysteresis loop F–x in the sense that it has its large axis making an angle less than 90° with respect to the x-axis in $\Omega < 1$ ante-resonance, and an angle greater than 90° in post-resonance for $\Omega > 1$. The elliptical Q–x hysteretic loops are tilted with their large axis only at angles below 90°. It can be noticed that the equality between the arias of the hysteretic loop, in the two representations systems Q–x and F–x, is verified, both being equal with the maximum dissipated energy $W_d^{\max}$.

Keywords: hysteretic loops; dissipated energy; linear dynamic systems

1. Introduction

For the vibration-driven technological processes with excitation harmonic forces, Voigt–Kelvin linear rheological models are adopted with the discretionary variation of the amortization or of the fraction of the critical amortization $\zeta = c/2\sqrt{k/m}$.

The functional optimization of the vibration-driven processes consists of reaching a maximum $W_d^{\max}$ dissipated energy for $\zeta = \zeta^0$ in direct correlation with the area of the elliptical hysteretic loop. By locating suitable transducers on the physical system, the elliptical hysteretic loops can be determined in such a manner that allows the assessment of their areas, respectively the maximum dissipated energy for a dynamic system may be assessed with rigidity k and amplitude A of the instantaneous displacement $x = A\sin(\omega t - \varphi)$, where φ is the phase angle.

Depending on the optimization requirement, in order to achieve a maximum dissipation, i.e., $W_d^{\max}$, can be determined the pairs of values $\zeta_{optim} = \zeta^0$ for which are established the calculus relations of the significant parameters. Thus, the functional relations were established for $A = A(\omega)$, amplitude, the $W_d = W_d(\zeta, \Omega)$ dissipated energy, the viscoelastic force $Q = c\dot{x} + kx = Q(x)$, and the excitation force $F = F(x)$. The correlations between the maximum dissipated energy and the areas of the elliptical hysteretic loops are reflected in the graphical representations for the case of operation in ante-resonance at $\Omega < 1$ and respectively for the case of post-resonance at $\Omega > 1$ [1–3].

Experimental research carried out so far has mainly highlighted the positioning of hysteretic loops as an ante-resonance regime for testing elastomeric devices. The results highlighted in this field, both linearly and nonlinearly, are presented in papers published by various researchers from Italy, France, USA, and Romania [4–10]. Interpretation of experimental results and behavioral modeling

of elastomeric device behavior are addressed in published reference works [11–18]. To highlight the post-resonance regime, interesting and useful research is contained in some published papers cited in the literature [19–23].

In this paper are highlighted the hysteretic loops families of the elastomeric devices that were designed, manufactured and tested, for a viaduct on the "Transilvania" Motorway, in Romania. Thus, based on dynamic testing devices and realized within ICECON Bucharest (Romania), there were determined the characeristic shapes of the hysteretic loops for the three dynamic regimmes, namely: ante-resonance, resonance, and post-resonance.

The characteristic function for dissipated energy was also established, highlighting its modification in relation to the fraction of critical damping ζ as a system parameter.

The novelty of the approach consists of the fact that for the elastomeric isolator system/device are highlighted the dissipative characteristics, the hysteretic loop orientation, as well as the dissipated energy variation depending on the parameter ζ, which can take different values in relation to mass m, elasticity k, and linear dissipation c. The graphical representation of the hysteretic loop in accordance with the dissipated energy allowed a clearer, more operational and efficient highlighting of the dynamic behavior during the tests, with meaningful and eloquent conclusions.

2. Parameter Analysis

The dynamic linear models m, c, and k, produced by the harmonic force $F(t) = F_0 \sin\omega t$ and with the reaction force $Q(t)$ in the liniar viscoelastic system, c, k, is presented in Figure 1.

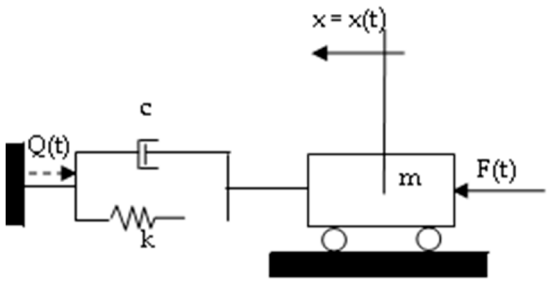

Figure 1. Linear dynamic model m, c, and k.

The movement equation at the dynamic balance is

$$m\ddot{x} + c\dot{x} + kx = F_0 \sin \omega t. \tag{1}$$

The solution of Equation (1) is

$$x = A \sin(\omega t - \varphi), \tag{2}$$

where A is the amplitude of the instantaneous displacement $x = x(t)$, φ is the phase shift between the instantaneous displacement $x(t)$ and the excitation force $F(t)$.

It is introduced the notation: $\Omega = \frac{\omega}{\omega_n}$, where $\omega_n = \sqrt{\frac{k}{m}}$, so that the variable Ω to be used as excitation relative pulsation.

2.1. Amplitude of Displacement

An amplitude of the instantaneous displacement $x = x(t)$ may be expressed by the $A(\omega)$ or $A(\Omega)$ relation, as follows:

$$A(\omega) = \frac{F_0}{\sqrt{(k - m\omega^2)^2 + c^2\omega^2}}, \tag{3}$$

or

$$A(\omega) = \frac{F_0}{k} \frac{1}{\sqrt{\left(1-\Omega^2\right)^2 + (2\zeta\Omega)^2}}. \tag{4}$$

2.2. De-Phasing between Force and Displacement

The de-phasing φ between the excitation force $F = F(t)$ and the instantaneous displacement $x = x(t)$ may be calculated as follows:

$$tg\varphi|_{\omega} = \frac{c\omega}{k - m\omega^2}, \tag{5}$$

or

$$tg\varphi|_{\Omega} = \frac{2\zeta\Omega}{1-\Omega^2}. \tag{6}$$

2.3. Dissipated Energy

The dissipated energy W_d may be expressed according to Ω and ζ as follows:

$$W_d = W_d(\Omega, \zeta) = W_0 \frac{2\zeta\Omega}{\left(1-\Omega^2\right)^2 + (2\zeta\Omega)^2}, \tag{7}$$

where $W_0 = \pi \frac{F_0}{k}$.

From the condition of maximum W_d, which is $\frac{dW_d}{d\zeta} = 0$, it emerges that $\zeta^0 = \pm\frac{1-\Omega^2}{2\Omega}$, so that the maximum dissipated energy $W_d^{\max}$ becomes

$$W_d^{\max} = W_0 \frac{1}{2(1-\Omega^2)} = W_0 \frac{1}{2(2\zeta\Omega)}. \tag{8}$$

It can be noticed that for certain values of Ω it correspond the values of ζ^0 for which the dissipated energy is at maximum. The representation of $W_d(\zeta)$, so that the variation domain of ζ to be included ζ^0, leads to a curve with a maximum point, having the coordinates ζ^0 at $W_d^{\max}$. For the discrete values of Ω, a family of parametrical curves of $W_d(\Omega, \zeta)$ can be obtained.

2.4. Equation of the F–x Elliptic Hysteretic Loop

Phase ωt is eliminated between $x = x(t)$ and $F = F(t)$ as follows:

$$\begin{cases} x = A\sin\omega t\cos\varphi - A\sin\varphi\cos\omega t \\ F = F_0\sin\omega t \end{cases}, \tag{9}$$

where $\sin\omega t = \frac{F}{F_0}$, $\cos\omega t = \pm\sqrt{1-\frac{F^2}{F_0^2}}$, resulting

$$\frac{x}{A} = \frac{F}{F_0}\cos\varphi \mp \sin\varphi\sqrt{1-\frac{F^2}{F_0^2}}. \tag{10}$$

If we note the dimensionless sizes $\frac{x}{A} = X$ and $\frac{F}{F_0} = \Phi$, then relation (10) becomes

$$X = \Phi\cos\varphi \mp \sin\varphi\sqrt{1-\Phi^2}. \tag{11}$$

From of equation (11) Φ emerges as

$$\Phi = X\cos\varphi \pm \sin\varphi\sqrt{1-X^2}, \tag{12}$$

where $\sin\varphi = \frac{c\omega}{\sqrt{(k-m\omega^2)^2+c^2\omega^2}}$ and $\cos\varphi = \frac{k-m\omega^2}{\sqrt{(k-m\omega^2)^2+c^2\omega^2}}$.

By replacing $\frac{x}{A} = X$, $\frac{F}{F_0} = \Phi$, $\sin\varphi$, and $\cos\varphi$ in relation (12), the expression of force F emerges according to pulsation ω, rigidity k, and amortization c as follows:

$$F(x) = F(x,\omega) = \left(k - m\omega^2\right)x \pm c\omega\sqrt{A^2(\omega) - x^2}, \tag{13}$$

or in terms of Ω and ζ measures we have

$$F(x,\Omega) = k\left[\left(1-\Omega^2\right)x \pm 2\zeta\Omega\sqrt{A^2(\Omega) - x^2}\right]. \tag{14}$$

For the condition that the dissipated energy to be maximum, $W_d = W_d^{\max}$ at $\zeta_{optim} = \zeta^0$.

(a) For the ante-resonance regime $\Omega < 1$ at $\zeta_a^0 = \frac{1-\Omega^2}{2\Omega}$, obtaining

$$F(x,\Omega) = \left(1-\Omega^2\right)k\left[x \pm \sqrt{A^2(\Omega) - x^2}\right], \tag{15}$$

or

$$F(x,\zeta,\Omega) = 2\zeta_a^0\Omega\, k\left[x \pm \sqrt{A^2\left(\Omega,\zeta_a^0\right) - x^2}\right]. \tag{16}$$

(b) For the post-resonance regime $\Omega > 1$ at $\zeta_p^0 = -\frac{1-\Omega^2}{2\Omega}$ the following is obtained:

$$F(x,\Omega) = \left(1-\Omega^2\right)k\left[x \pm \sqrt{A^2(\Omega) - x^2}\right], \tag{17}$$

or

$$F(x,\zeta,\Omega) = -2\zeta_p^0\Omega k\left[x \pm \sqrt{A^2\left(\Omega,\zeta_p^0\right) - x^2}\right]. \tag{18}$$

where

$$A(\Omega) = \pm\frac{F_0}{k}\frac{1}{(1-\Omega^2)\sqrt{2}}, \tag{19}$$

or

$$A\left(\Omega,\zeta_{a,p}^0\right) = \pm\frac{F_0}{k}\frac{1}{2\zeta_{a,p}^0\Omega\sqrt{2}}. \tag{20}$$

2.5. Equation of the Hysteretic Loop Q–x

The instantaneous viscous-elastic force $Q(t) = c\dot{x} + kx$ may be expressed from the dynamic equilibrium equation. Thus, it can be expressed $m\ddot{x} + c\dot{x} + kx = F(t)$ or

$$m\ddot{x} + Q(t) = F(t), \tag{21}$$

from where $Q(t)$ emerges as $Q(t) = F(t) - m\ddot{x}$, or in relation with $x = x(t)$, it is obtained

$$Q(x) = F(x) - m\left(-\omega^2 x\right). \tag{22}$$

In Equation (22) we insert the expression of force $F(x) = F(x,\omega)$ from (13) and have

$$Q(x) = Q(x,\omega) = kx \pm c\omega\sqrt{A^2(\omega) - x^2}, \tag{23}$$

and in relation with Ω Equation (23) becomes

$$Q(x) = Q(x, \omega) = k\left[x \pm 2\zeta\Omega\sqrt{A^2(\Omega) - x^2}\right]. \quad (24)$$

It is found that the family of ellipses according to Equation (24) is characterized by the fact that all ellipses have their major axis in the quadrant $(0, \pi/2)$ with positive angular coefficient $tg\alpha = k > 0$ for any value $\Omega > 0$, where α is the angle between the ellipse axis and the Ox axis [24].

3. Elliptic Hysteretic Loops for the Ante-Resonance Regime ($\Omega < 1$)

For a dynamic system where $m = 10^4$ kg, $k = 2{\cdot}10^7$ N/m at the relative pulses $\Omega_1 = 0.8$ with $\zeta_{optim} = \zeta_1^0 = 0.225$; $\Omega_2 = 0.6$ with $\zeta_{optim} = \zeta_2^0 = 0.53$; and $\Omega_3 = 0.5$ with $\zeta_{optim} = \zeta_3^0 = 0.75$, the representation of the elliptical hysteretic loops Q–x and F–x, according to the graph of function $W_d = W(\zeta)$, as shown in Figures 2–4. In each figure functions $F(x)$ and $Q(x)$ are represented based on Equations (16) and (24), respectively, corresponding to the representation of function $W_d{}^{max} = W(\zeta)$, given by Equation (8). Thus, it is found that for the maximum value of the dissipated energy $W_d{}^{max}$ according to $\Omega_i < 1$ and $\zeta_{optim} = \zeta_i^0$, $i = 1, 2, 3$, the areas of the ellipses F–x and Q–x are maximum and equal [25–29]

We specify the fact that the fraction of the critical amortization ζ_{ef}, in this case for $W_d{}^{\max}$, may be defined as follows:

$$\zeta_{ef} = \frac{W_d^{\max}}{4\pi\frac{1}{2}kA^2(\omega, \zeta^0)}, \quad (25)$$

and taking into account Equations (8) and (20), we have

$$\zeta_{ef} = \zeta^0\Omega. \quad (26)$$

It can be observed that only at a resonance, when $\Omega_i = 1$, it results $\zeta_{ef} = \zeta^0$.

In Figures 2–5, the functions $W_i = W_i(\zeta)$, F_i–x, and Q_i–x are represented for $\zeta_{optim} = \zeta_i^0$ in which $W_i = W_d{}^{\max}(\zeta^0)$ and Ω_i where $i = 1, 2, 3$.

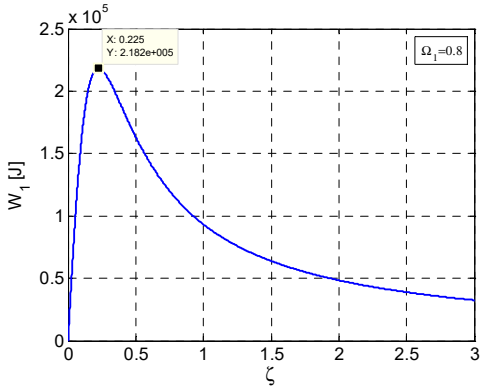

(**a**): $W_{1\,max} = 2.1{\cdot}10^5$J

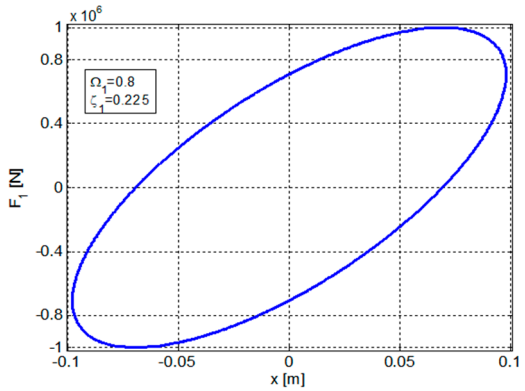

(**b**): area = $2.1{\cdot}10^5$ J

Figure 2. *Cont.*

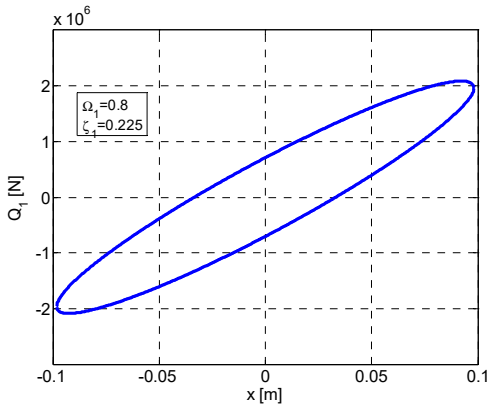

(**c**): area = 2.1·10^5 J

Figure 2. Variation curves in ante-resonance for $W_1{}^{max}$ at $\Omega_1 = 0.8$ and $\zeta_1 = 0.225$. (**a**) Variation of W_1 according to ζ. (**b**) Elliptic hysteretic loop F_1–x. (**c**) Elliptic hysteretic loop Q_1–x. x = [−0.08701 ÷ +0.08701].

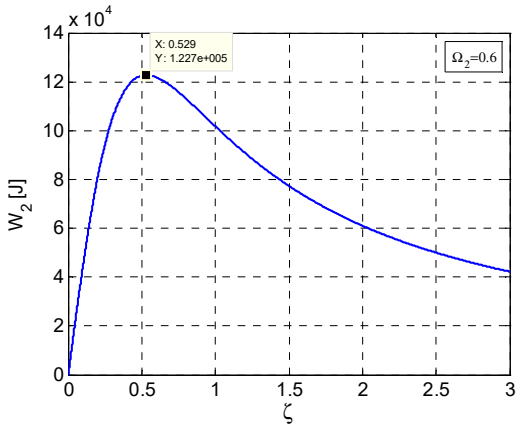

(**a**): $W_{2\,max}$ = 1.2·10^{5}J

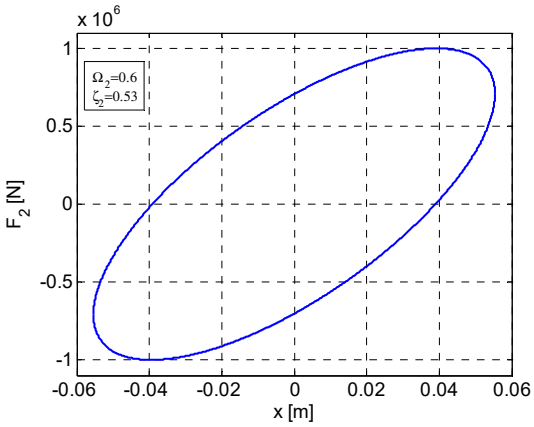

(**b**): area = 1.2·10^5 J

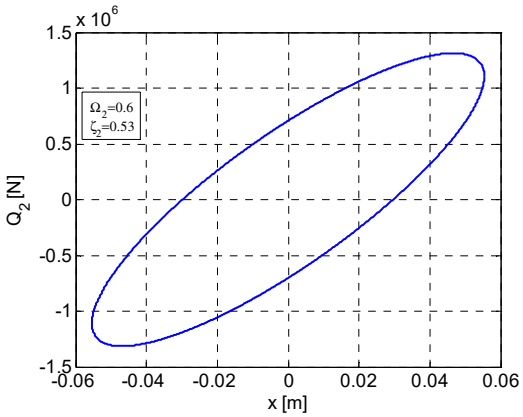

(**c**): area = 1.2·10^5 J

Figure 3. Variation curves in ante-resonance for $W_2{}^{max}$ at $\Omega_2 = 0.6$ and $\zeta_2 = 0.53$. (**a**) Variation of W_2 according to ζ. (**b**) Elliptic hysteretic loop F_2–x. (**c**) Elliptic hysteretic loop Q_2–x. x = [−0.05542 ÷ +0.05542].

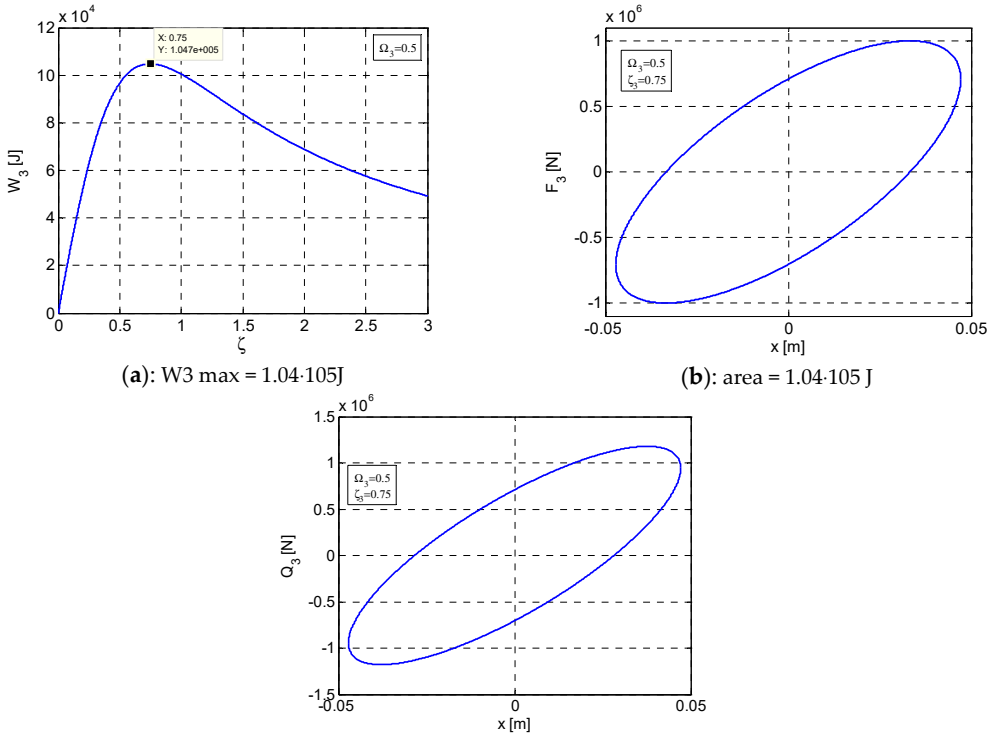

(**a**): W3 max = 1.04·105J (**b**): area = 1.04·105 J

(**c**): area = 1.04·105 J

Figure 4. Variation curves in ante-resonance for $W_3{}^{max}$ at $\Omega_3 = 0.5$ and $\zeta_3 = 0.75$. (**a**) Variation of W_3 according to ζ. (**b**) Elliptic hysteretic loop F_3–x. (**c**) Elliptic hysteretic loop Q_3–x. $x = [-0.04715 \div +0.04715]$.

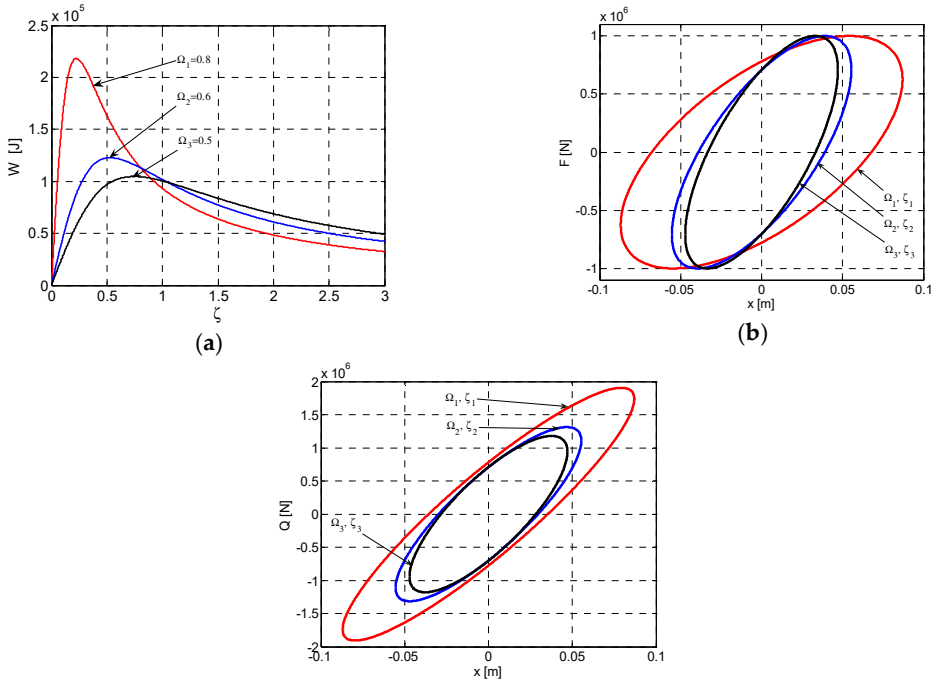

(**a**) (**b**)

(**c**)

Figure 5. Families of curves in ante-resonance for $W_1{}^{max}$, $W_2{}^{max}$, and $W_3{}^{max}$. (**a**) Families of curves W according to the current variable ζ and the discreet variable Ω. (**b**) The family of elliptical hysteretic loops F–x according to the current variable x and the pair of discreet variables Ω, ζ. (**c**) The family of elliptical hysteretic loops Q–x according to the current variable x and the pair of discreet variables Ω, ζ.

4. Elliptic Hysteretic Loops for the Post-Resonance Regime ($\Omega > 1$)

In the case of the above described system, for Ω_4 = 1.31 with $\zeta_4^0 = 0.28$; Ω_5 = 1.66 with $\zeta_5^0 = 0.53$; Ω_6 = 2 with $\zeta_6^0 = 0.75$, and Ω_7 = 2.32 with $\zeta_7^0 = 0.95$, in the Figures 6–10 there were represented the functions $W_i(\zeta)$ and $Q_i(x)$ were i = 4,5,6,7.

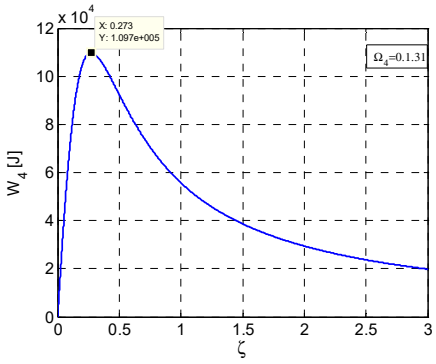

(**a**): $W_{4\,max}$ = 1.09·10^{5}J

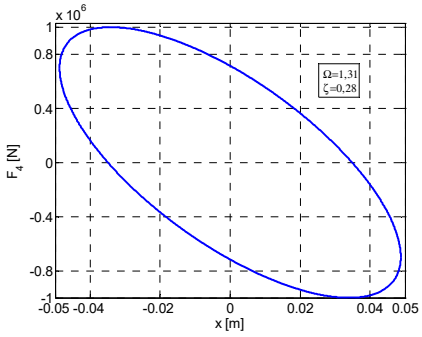

(**b**): area = 1.09·10^5 J

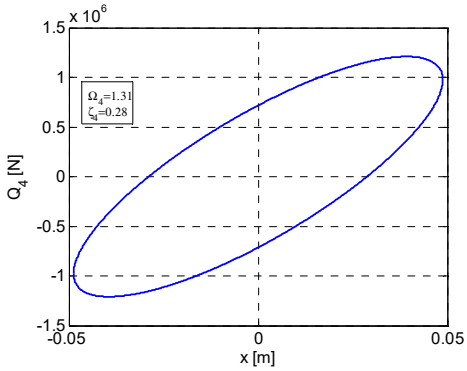

(**c**): area = 1.09·10^5 J

Figure 6. Variation curves in post-resonance for $W_4{}^{max}$ at Ω_4 = 1.31 and ζ_4 = 0.28. (**a**) Variation of W_4 according to ζ. (**b**) Elliptic hysteretic loop F_4–x. (**c**) Elliptic hysteretic loop Q_4–x. x = [−0.04878 ÷ +0.04878].

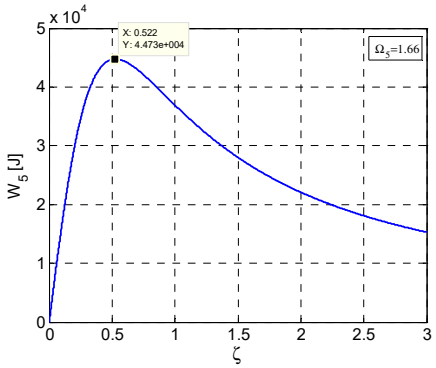

(**a**): $W_{5\,max}$ = 4.47·10^{4}J

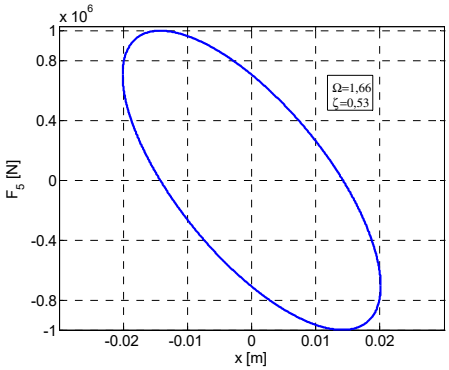

(**b**): area = 4.47·10^4 J

Figure 7. *Cont.*

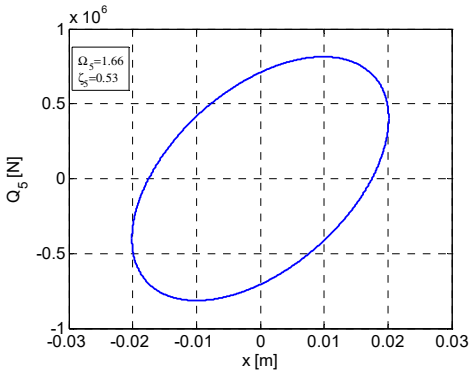

(**c**): area = 4.47·10⁴ J

Figure 7. Variation curves in post-resonance for W_5^{max} at $\Omega_5 = 1.66$ and $\zeta_5 = 0.53$. (**a**) Variation of W_5 according to ζ. (**b**) Elliptic hysteretic loop F_5–x. (**c**) Elliptic hysteretic loop Q_5–x. $x = [-0.02012 \div +0.02012]$.

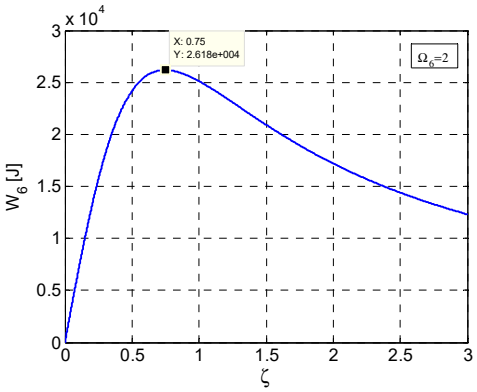

(**a**): $W_{6\,max} = 2.61 \cdot 10^4$J

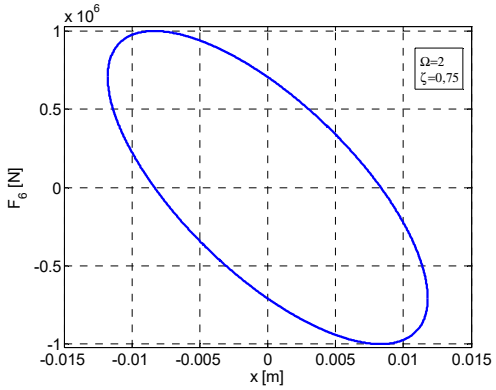

(**b**): area = 2.61·10⁴ J

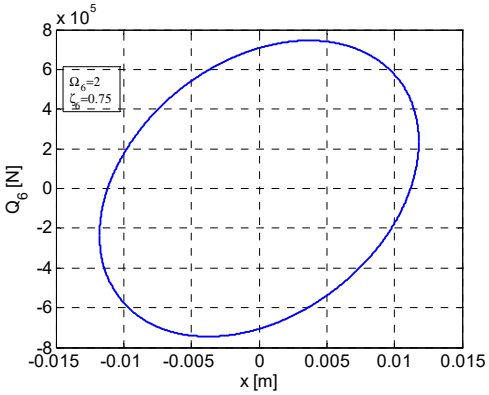

(**c**): area = 2.61·10⁴ J

Figure 8. Variation curves in post-resonance for W_6^{max} at $\Omega_6 = 2$ and $\zeta_6 = 0.75$. (**a**) Variation of W_6 according to ζ. (**b**) Elliptic hysteretic loop F_6–x. (**c**) Elliptic hysteretic loop Q_6–x. $x = [-0.01179 \div +0.01179]$.

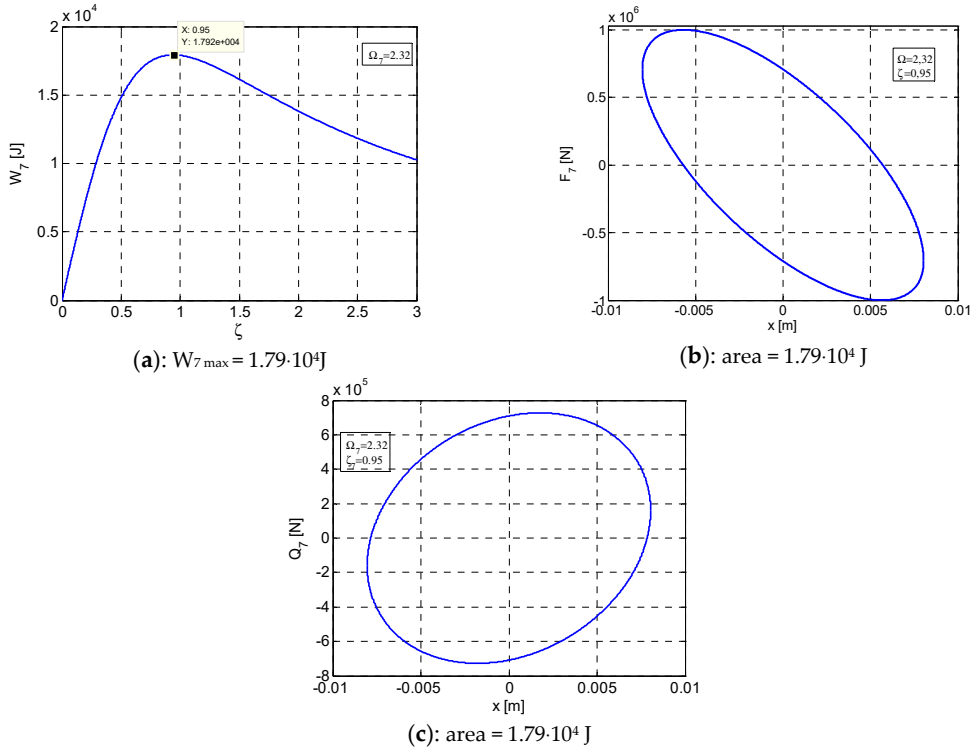

Figure 9. Variation curves in post-resonance for W_7^{max} at $\Omega_7 = 2.32$ and $\zeta_7 = 0.95$. (**a**) Variation of W_7 according to ζ. (**b**) Elliptic hysteretic loop F_7–x. (**c**) Elliptic hysteretic loop Q_7–x. $x = [-0.008045 \div +0.008045]$.

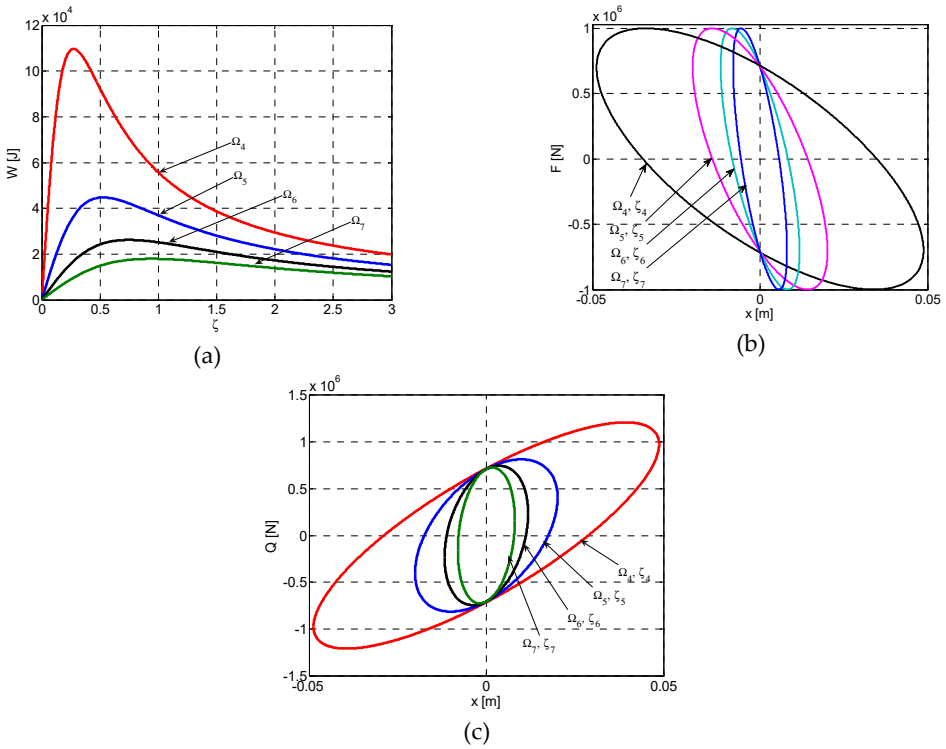

Figure 10. Families of curves in post-resonance for the maximum values of the dissipated energy W_4, W_5, W_6, and W_7 at parameters (Ω_4, ζ_4), (Ω_5, ζ_5), (Ω_6, ζ_6), and (Ω_7, ζ_7). (**a**) Families of curves W parametrized by the discreet variable Ω. (**b**) The family of elliptical hysteretic loops F–x for the pair of variables Ω, ζ. (**c**) The family of elliptical hysteretic loops Q–x for the pair of variables Ω, ζ.

5. Conclusions

The dynamic linear system m, c, and k excited by a harmonic perturbatory force is assessed dynamic regimes of ante-resonance $\Omega < 1$ and and post-resonance $\Omega > 1$ for values of the viscous dumping $\zeta = \zeta_{optim} = \zeta^0$, for which the dissipated energy is maximum: $W_d = W^{\max}(\zeta^0)$.

(a) For this, there are established the functional relations of the perturbatory force $F = F(x)$ in relation with the instantaneous displacement $x = x(t)$, of the viscoelastic force $Q = Q(t)$ in relation with $x = x(t)$, of the viscoelastic force $Q = Q(x)$ in relation with $x = x(t)$, and of the dissipated energy in relation with the variation of the viscous dumping ζ, namely $W_d = W(\zeta)$;

(b) In this context, based on the graphical representations, it was possible to emphasize the fact that the ellipses F–x are rotating in relation to the origin of the axis system, according to the dynamic regime $\Omega < 1$ or $\Omega > 1$. The axis of the ellipse F–x rotation is caused by the inertial effect that is produced by the presence of the factor $1 - \Omega^2$ in the expression of the function $F = F(x)$;

(c) The representation of the function $Q = Q(x)$ highlights the that it constantly maintains an angle of inclination of the ellipse Q–x, axis, with a positive slope;

(d) It can be noticed that the areas of the hysteretic loops F–x and Q–x are equal between them and equal with the maximum value of the dissipated energy $W^{\max}(\zeta^0)$ for $\zeta^0 = \frac{1-\Omega^2}{2\Omega}$.

(e) The effective critical dumping ζ_{ef} depends both on the value of ζ^0 as well as on the relative pulsation $\Omega < 1$, for ante-resonance or $\Omega > 1$, for post-resonance. In the case of the resonance regime, for $\Omega = 1$, then $\zeta_{ef} = \zeta^0$ is a sole situation that enables the assessment of the fraction from the optimal critical amortization ζ^0.

The concordant graphical representations eloquently demonstrated the fact that for the dynamic regimes defined by the relative pulsation Ω, the dissipative effects of the linear viscous-elastic systems may be analyzed, in experimental conditions defined by specific requirements.

The obtained results are based on the experimental tests performed on dynamic testing systems using real manufactured products. The tests were carried out in laboratories specialized in the testing of anti-vibration and anti-seismic devices, and the devices, belonging to recognized laboratories or manufacturing companies such as SISMALAB (Italy), EUCENTRE (Italy), DIS (Reno, USA), ALGA (Italy), and ICECON (Romania).

Based on the researches and the results presented in this paper, were designed and manufactured the elastomeric anti-seismic devices used for a viaduct with a length of 200 m, on the "Transilvania" Motorway, constructed by the Bechtel company (USA), in Romania.

The experimental tests performed in order to determine the hysterical loop families were conducted within the ICECON Romanian Research Institute for Construction Equipment and Technology – ICECON, using both anti-vibration and anti-seismic devices.

The assessment system using specialized tests was based on the Romanian Patent No. 80484/1982 "Stand for the measurement of the mechanical characteristics of rubber", whose owner is the author of this paper.

Funding: This research received no external funding.

Conflicts of Interest: The authors declare no conflict of interest.

References

1. Dobrescu, C. The Rheological Behaviour of Stabilized Bioactive Soils During the Vibration Compaction Process for Road Structures. In Proceedings of the 22th International Congress on Sound and Vibration, Florence, Italy, 12–16 July 2015.
2. Mitu, A.M.; Sireteanu, T.; Ghita, G. Passive and semi-active bracing systems for seismic protection: A comparative study. *Rom. J. Acoust. Vib.* **2015**, *12*, 49–56.
3. Sireteanu, T. Smart suspension systems. *Rom. J. Acoust. Vib.* **2016**, *13*, 2.

4. Conveney, V.V.; Johnson, D.E.; Kulak, R.F. Modelling the Free Oscillation of Building Suported on High Damping Rubber Isolators. In Proceedings of the Seismic Engineering 2000, The 2000 ASME Pressure Vessels and Piping Conference, Seattle, WA, USA, 23–27 July 2000; Volume 1.
5. Lin, S.B. Theoretical and Experimental Study of High Damping Rubber Bearing and Lead Extrusion Damper. Master's Thesis, Feng Chia University, Taichung, Taiwan, 2000.
6. Chen, B.J.; Lin, S.B.; Tsai, C.S. Theoretical and Experimental Study of High Damping Rubber Bearings. In Proceedings of the Seismic Engineering 2001, The 2000 ASME Pressure Vessels and Piping Conference, Seattle, WA, USA, 23–27 July; Volume 2.
7. Dolce, M.; Ponzo, F.C.; Di Cesare, A.; Arlego, G. *Progetto di Edifici con Isolamento Sismico*; IUSS Press: Pavia, Italy, 2010.
8. Marioni, A. Sisitemi di Isplamento Sismico Innovetivi Prodotti dalla Societa ALGA. In *Moderni Sistemi e Tecnologie Antisismici. Una Guida per il Progettista*; 21mo Secolo: Milano, Italy, 2008.
9. Bratu, P. Vibration Transmissivity in Mechanical Systems with Rubber Elements Using Viscoelastic Models. In Proceedings of the 5th European Rheology Conference, Ljubljana, Slovenia, 6–11 September 1998.
10. Delfosse, C.G. Étude des vibrations linéaires d'un systeme mecanique complexe par méthode des mates normaux. *Ann. l'ITBTP* **1976**, *336*, 122–136.
11. Giacchetti, R. *Fondamente di Dinamica delle Strutture e di Ingineria Sismica*; EPC Libri: Roma, Italy, 2004.
12. Bratu, P. Analyze Insulator Rubber Elements Subjected to Actual Dynamic Regime. In Proceedings of the 9th International Congress Sound and Vibration, Orlando, FL, USA, 8–11 July 2002.
13. Bratu, P. Experimental evaluation of the antivibrating damping capacity in case of elastomers used for tram railway supportins. *Mater. Plast.* **2009**, *46*, 127–130.
14. Bratu, P. Rheological model of the neopren elements used for base isolation against seismic actions. *Mater. Plast.* **2009**, *46*, 288–294.
15. Jennings, P. Equivalent viscous damping for yelding structures. *J. Eng. Mech. Division* **1968**, *94*, 103–116.
16. Rao, M. *Mechanical Vibrations*; Addison-Wesley Pub. Co.: Boston, MA, USA, 2011.
17. Sireteanu, T.; Giuclea, M.; Mitu, A.M. An analitical approach for approximation of exxperimental hysteretic by Bouc.-Wen model. *Procc. Rom. Acad. Ser. A* **2009**, *10*, 4354.
18. Sireteanu, T.; Giuclea, M.; Mitu, A.M. Identification of an extended Bouc.-Wen model with application to seismic protection through hysteretic devices. *Comput. Mech.* **2010**, *45*, 5. [CrossRef]
19. Le Tallec, P. *Introduction à la Dynamique des Structures*; Cépaduès: Toulouse, France, 2000.
20. Trigili, G. *Introduzione alla Dinamica delle Strutture e Spettri di Progeto*; Laccorio: Palermo, Italy, 2010.
21. Dolce, M.; Mortelli, A.; Panza, G. *Proteggersi dal Terremoto*; 21/mo Secolo: Milano, Italy, 2004.
22. Mortelli, A.; Sannino, U.; Parducci, A.; Braga, F. *Moderni Sistemi e Tecnologie Antisismici Una Guida per il Progettista*; 21mo Secolo: Milano, Italy, 2008.
23. Radeș, M. *Mechanical Vibrationes*; Ed. Printech: București, Romania, 2006.
24. Johnson, E.A.; Ramallo, J.C.; Spencer, B.F., Jr.; Sain, M.K. Intelligent Base Isolation Systems. In Proceedings of the 2nd World Conference on Structural Control, Kyoto, Japan, 28 June–1 July 1998.
25. Wang, Y.-P. Fundamentals of Seismic Base Isolation. In *International Training Programs for Seismic Design of Building Structures*; National Certer of Research on Earthquake Engineering: Taipei, Taiwan, 2016.
26. Stanescu, N.D. Vibrations of a shell with clearances, neo-Hookean stiffness, and harmonic excitations. *Rom. J. Acoust. Vib.* **2016**, *13*, 104–111.
27. Vasile, O. Active vibration control for viscoelastic damping systems under the action of inertial forces. *Rom. J. Acoust. Vib.* **2017**, *14*, 54–58.
28. Inman, D. *Vibration with Control*; John Wiley & Sons Ltd.: London, UK, 2007.
29. Najari, S. *Identification par Analyse Harmonique des Structures en Géniè Civil*; INSA: Toulouse, France, 1981.